

# Intermediate Cu-O-Si Phase in the Cu-SiO<sub>2</sub>/Si(111) System: Growth, Elemental, and Electrical Studies

Reshmi Sreedharan, Manu Mohan, Sonia Saini, Anupam Roy, and Kuntala Bhattacharjee\*

Cite This: *ACS Omega* 2021, 6, 23826–23836

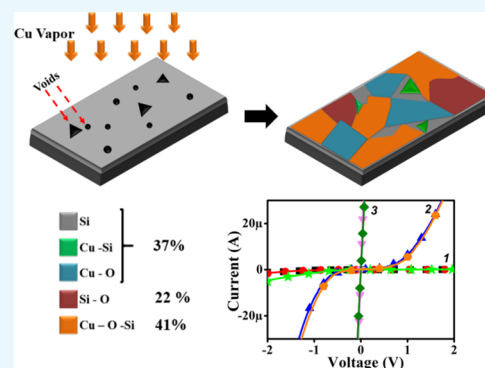
Read Online

ACCESS |

Metrics &amp; More

Article Recommendations

**ABSTRACT:** We investigate here the strain-induced growth of Cu at 600 °C and its interactions with a thermally grown, 270 nm-thick SiO<sub>2</sub> layer on the Si(111) substrate. Our results show clear evidence of triangular voids and formation of triangular islands on the surface via a void-filling mechanism upon Cu deposition, even on a 270 nm-thick dielectric. Different coordination states, oxidation numbers, and chemical compositions of the Cu-grown film are estimated from the core level X-ray photoelectron spectroscopy (XPS) measurements. We find evidence of different compound phases including an intermediate mixed-state of Cu–O–Si at the interface. Emergence of a mixed Cu–O–Si intermediate state is attributed to the new chemical states of Cu<sup>x+</sup>, O<sup>x</sup>, and Si<sup>x+</sup> observed in the high-resolution XPS spectra. This intermediate state, which is supposed to be highly catalytic, is found in the sample with a concentration as high as ~41%. Within the Cu–O–Si phase, the atomic percentages of Cu, O, and Si are ~1, ~86, and ~13%, respectively. The electrical measurements carried out on the sample reveal different resistive channels across the film and an overall n-type semiconducting nature with a sheet resistance of the order of 10<sup>6</sup> Ω.



## 1. INTRODUCTION

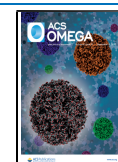
The study of metal, silicon (Si) interactions,<sup>1–9</sup> and formation of interface is important owing to its application in the electronics and semiconductor industry.<sup>10–12</sup> With Si-based technologies still governing the integrated circuits, the Cu–Si system has been of particular importance in delivering promising applications from silicon bronzes to catalysis,<sup>12–21</sup> microelectronics,<sup>22</sup> Li-ion batteries,<sup>23,24</sup> solar cells,<sup>25–29</sup> and more. Copper (Cu) with its low cost, low electrical resistivity (~1.7 μΩ cm), high melting point (1357.6 K), and low diffusivity showed tremendous potential over aluminum for applications in the electronic devices such as Schottky junctions,<sup>30</sup> metal gates<sup>31</sup> and local interconnects.<sup>11,32</sup> However, even with a low diffusivity, Cu interacts with the Si or SiO<sub>2</sub>/Si substrate, making it a limiting factor for the device performances due to the problem of leakage current. Pavlenko and Cherkashina have particularly investigated the stability of the grown composite films on the SiO<sub>2</sub> layer.<sup>33</sup> Many studies have been carried out to understand Cu growth on the SiO<sub>2</sub>/Si matrix,<sup>31,34</sup> or on the native oxide of the Si substrate.<sup>11,35–40</sup> Zhang et al.<sup>40</sup> have reported shape- and orientation-controlled growth of nanotriangles, nanosquares, and nanowires of Cu<sub>3</sub>Si on a 2–4 nm-thick native SiO<sub>2</sub> layer on Si(111), Si(100), and Si(110) surfaces, respectively, through a Au nanoparticle-assisted vapor transport method and reviewed the dependence of substrate crystal symmetry on the growth morphology of Cu<sub>3</sub>Si. Cemin et al.<sup>41</sup> have demonstrated the growth of epitaxial ultrathin Cu films of up

to 150 nm at ambient temperature conditions using high power impulse magnetron sputtering and substrate biasing on the native oxide-covered Si(001) oriented substrate. According to their report,<sup>41</sup> the heteroepitaxial growth of Cu(001) on the Si(001) with the native oxide occurred via the formation of a complex interface composed of various copper silicides and amorphous phases.

The effect of annealing on the Cu–Si system had been studied by different groups.<sup>1,38,42,43</sup> Thin films deposited at room temperature (RT) by thermal evaporation usually do not form good chemical bond with the substrate due to the lower kinetic energy of the incoming atoms and non-uniformity in the sticking coefficient.<sup>44</sup> Growth at an elevated temperature and post-deposition annealing are important processes to achieve high-quality films from the vapor deposition technique; however, they can lead to the formation of silicides and oxides in the case of the Cu–SiO<sub>2</sub>/Si system. The coefficient of Cu segregation in a clean Si(111) surface without any oxide layer is reported to be highest for a temperature range of 500–650 °C.<sup>43</sup> Annealing will lead to the coalescence of copper and

Received: May 20, 2021

Published: September 8, 2021



formation of isolated crystallites,<sup>40</sup> which are mostly composed of copper silicide on the native oxide of 2–4 nm on bare Si substrates. As a result, these nanostructures usually follow the crystal symmetry of the substrate surface.

The diffusion and interaction of Cu in the SiO<sub>2</sub>/Si system will mainly result in the formation of Cu silicides and Cu oxides depending on growth parameters and thickness of the SiO<sub>2</sub> layer. By performing Rutherford backscattering experiments on the Cu/Si system, Sekar et al. had shown that for Si(111) surfaces with a native oxide layer, the onset temperature of interdiffusion of Cu is in the range of 500–700 °C.<sup>1</sup> Cu silicides can form at a relatively lower temperature than other metal silicides.<sup>45</sup> Three stable Cu–Si alloys exist at RT and are metallic. Out of them, Cu<sub>3</sub>Si is the most stable.<sup>11</sup> Cu silicides have got significant applications as a catalyst for hydrogenation,<sup>20</sup> chlorosilane formation,<sup>46</sup> and gas etching of silicon.<sup>47</sup> Strong resistance to oxidation is displayed by these metal silicides compared to their metal counterparts, which makes them highly applicable as electronic interconnects. Owing to its high charging and optimized cycling properties, the metallic Cu<sub>3</sub>Si poses itself as a suitable candidate as an anode in lithium-ion batteries.<sup>48</sup> On the other hand, the two main variants of Cu oxides, which are usually formed due to the reaction with oxygen from the SiO<sub>2</sub> interface, are Cu<sub>2</sub>O and CuO. Both these oxides are p-type semiconductors. Cu oxide thin films have been widely studied in the past decades where it has been shown that Cu<sub>2</sub>O is a good candidate for applications in the area of spintronics,<sup>49</sup> catalysis,<sup>50</sup> and solar cells,<sup>51,52</sup> whereas CuO is an attractive system related to photothermal and photoconductive applications.<sup>53</sup> Also, the highly catalytic property of the Cu/SiO<sub>2</sub> system<sup>13–16</sup> is likely to promote metal–support interaction via controlling the catalysis of the metal particles. An intermediate Cu–O–SiO<sub>x</sub> phase in the Cu/SiO<sub>2</sub> interface is reported to exhibit extraordinary catalytic activity to dissociate H<sub>2</sub> for hydrogenation of esters.<sup>20</sup> SiO<sub>2</sub>-coated Cu nanocatalysts with a very active and abundant Cu–O–SiO<sub>x</sub> interface is responsible to assist the huge selective hydrogenation of dimethyl oxalate that is about 80 times more than that of pristine Cu at the temperature range between 200–240 °C.<sup>20</sup>

The work presented here is greatly motivated by the scientific importance and wide range of applications displayed by the Cu–SiO<sub>2</sub>/Si system in different areas starting from electronic devices to catalysis. Though, the Cu–Si system had been widely studied earlier from the morphological,<sup>40,41</sup> compositional,<sup>31,34,54–56</sup> electronic, and electrical transport<sup>45,54,57</sup> aspects, a comprehensive and systematic study related to the growth and interaction of Cu into a large SiO<sub>2</sub> barrier was missing, which is important to address the underlying issues related to micro- and nanoelectronics, energy storage, solar cells, and catalysis. In this work, we aim to study this atypical Cu–SiO<sub>2</sub>/Si system from a more general perspective to illustrate the growth, elemental compositions, and electrical nature of the film when Cu was grown on a 270 nm-thick SiO<sub>2</sub> dielectric on the Si(111) substrate at 600 °C and was annealed post-deposition at the same temperature for 1 h. The formation of different Cu-induced phases in the SiO<sub>2</sub>/Si matrix would depend on the temperature, thickness of the SiO<sub>2</sub> barrier, diffusion processes, chemical reactivity of the atoms, and amount of the deposited material. The surface morphology and elemental compositions of the grown film were studied by using atomic force microscopy (AFM), scanning electron microscopy (SEM), and X-ray photoelectron

spectroscopy (XPS). AFM and SEM measurements provide direct evidence of triangular voids and formation of islands via a void-filling mechanism upon Cu deposition on the surface. XPS analyses reveal the appearance of a highly catalytic Cu–O–Si intermediate phase that is present in the film with highest concentration (~41%) in addition to other compound phases. The elemental compositions of the intermediate state were calculated to be ~1, ~86, and ~13% for Cu, O, and Si, respectively. Electrical characterizations were performed in a two probe transport measurement system using van der Pauw (vdP) geometry in the presence of a magnetic field applied perpendicular to the plane of the sample. The results disclose an n-type semiconducting behavior of the film with a sheet resistance of the order of 10<sup>6</sup> Ω. We present here our classified experimental observations on the Cu–SiO<sub>2</sub>/Si system that might provide useful and effective insights to address future scientific interest related to this topic.

## 2. EXPERIMENTAL TECHNIQUES

Si (111) substrates with a SiO<sub>2</sub> layer of 270 nm thickness were purchased from Testbourne Ltd., UK. SiO<sub>2</sub>/Si (111) wafers were initially cleaned in organic solvents before loading into the deposition chamber. The turbomolecular pump-based thermal evaporation setup was procured from H. Fillunger and Co. Pvt. Ltd. Pune, India. In the thermal deposition chamber, the substrate temperature was set and maintained at 600 °C by a temperature controller for 60 min before the deposition to ensure uniform temperature attainability of the substrate surface. The temperature of the substrate heater was measured by a thermocouple, and the set temperature of 600 °C of the substrate heater was maintained within an accuracy of ±10 °C. Copper was deposited from a thermal evaporator for 30 s at a rate of 2 Å/s on the SiO<sub>2</sub>/Si (111) surface. The base pressure inside the chamber before deposition was of the order of 10<sup>–5</sup> Pa, whereas during deposition, it was around 5.7 × 10<sup>–4</sup> Pa. After deposition, the substrate heater was maintained at the same temperature of 600 °C for 60 min to anneal the samples. Post-deposition annealing was followed by normal cooling down of the samples to RT before taking them out from the growth chamber.

The surface morphology of the samples was investigated using AFM in tapping mode (Agilent: 5500 AFM/SPM N9410S and Nanosurf: NiaoAFM) and SEM (Carl Zeiss EVO 18 secondary electron microscope). The SEM images were acquired at an operating voltage of 5 kV. Data acquired by AFM were investigated and analyzed using the WSxM<sup>58</sup> software package, and SEM images were analyzed using ImageJ. The elemental composition and chemical stoichiometry of the samples were studied by XPS. All XPS spectra were acquired at room temperature using an Omicron Multiprobe system and monochromatic Al–Kα ( $h\nu = 1486.7$  eV) X-ray radiation source.<sup>59</sup> The background pressure during measurements was kept below 3 × 10<sup>–8</sup> Pa, and the pass energy for the high-resolution spectra was 20 eV. A CN10 charge neutralizer was used to compensate for the charging effect during the measurement, and the samples were not ion-sputtered before the measurement. The binding energies of all the registered XPS spectra have been calibrated to the C–C component of the C 1s peak, which is at 284.8 eV. However, this method of referencing that corresponds to adventitious carbon contaminations might be erroneous as the elemental composition and thickness of the film vary.<sup>60</sup> The chemical composition of the grown film was quantified using the Casa XPS software. In the

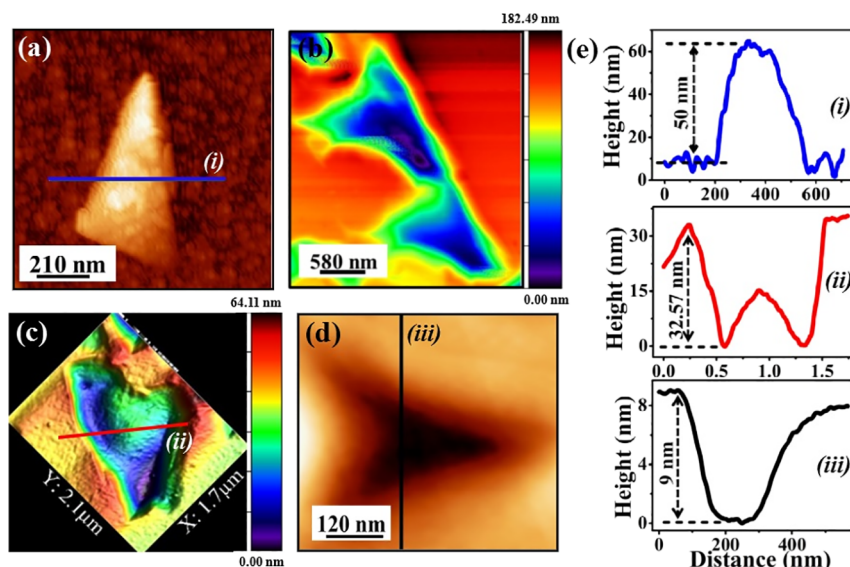


**Figure 1.** AFM images of Cu-deposited film on the SiO<sub>2</sub>/Si(111) surface (a–d). Height profiles taken along the corresponding lines (marked as (i–iii) in (a–d)) are shown in (e).

deconvolution process, some of the peak parameters like binding energy, FWHM, peak area, etc., were kept fixed<sup>61</sup> and the fitting of the spectra were performed using either a combination of the Gaussian/Lorentzian function with GL line shapes (with varying FWHM for component peaks) or with the Voigt function following a Shirley background correction. The percentage elemental compositions of the Cu–O–Si phase are obtained from the equation:

$$X_j = \frac{A_j/S_j}{\sum_i (A_i/S_i)} \quad (1)$$

where  $X_j$  is the atomic concentration of element  $j$ ,  $A_j$  is the peak area, and  $S_j$  is the sensitivity factor of the element  $j$  given in the XPS analysis software.<sup>62</sup>

Raman spectroscopy measurements have been carried out in a Renishaw inVia Raman microscope using a laser excitation of 532 nm. The electrical characterizations have been performed using a two-probe probe station connected to an Agilent B2912A precision source/measure unit. RT Hall measurements were made in vdP geometry at high vacuum conditions in a direct current probe station with an integrated PM5. A magnetic field of strength 1.0 T was applied perpendicular to the sample surface. The system was coupled with an Agilent semiconductor device analyzer B1500A.

### 3. RESULTS AND DISCUSSIONS

**3.1. Morphology: AFM and SEM Investigations.** Figure 1 shows AFM investigations of the surface morphology of a 30 s Cu-deposited film on a SiO<sub>2</sub>/Si (111) substrate. It can be seen that Cu grows as a triangular island (Figure 1a) with side lengths in the range of 300–500 nm. The profile (Figure 1e) taken along the line (i) marked in the image shows the height of the island, which is around 50 ± 10 nm. According to Zhang et al., the growth of Cu at 600 °C may not be a single crystal.<sup>40</sup> This is clear from the AFM image shown in Figure 1a, where the surface seems to be uneven or rough signaling mostly a polycrystalline nature of the film.<sup>40</sup> A detailed investigation of the sample further reveals the formation of triangular voids (Figure 1b–d) with varying dimensions on the surface. Small

triangular voids (Figure 1d) have side lengths approximately 100 nm, whereas large triangular voids (Figure 1b,c) exhibit side lengths in the range between 1.0 and 2.0 μm. Depth of the triangular voids varies from a few (~10) nm for small ones to 100–200 nm for large ones as revealed by AFM micrographs (Figure 1b–d). Evidence of empty (Figure 1b,d) and partially filled triangular (Figure 1c) voids are also clearly seen in the AFM measurements. The line profiles taken across the voids (marked as (ii) and (iii)) are shown in Figure 1e. From various AFM images, we have tried to find out the number density of such voids, which is 1–3 voids/100 μm<sup>2</sup>. The occurrence of empty or partially filled voids is an indication of the rapid growth of voids in the system. The growth of such triangular voids following substrate crystal symmetry and growth of Cu on a relatively thick SiO<sub>2</sub>/Si is not yet reported.

The formation of voids and the growth of Cu silicides through void-filling mechanisms were explored by Li and his coworkers.<sup>11</sup> They reported the growth of voids from the defect sites that are already present at the thermally grown SiO<sub>2</sub> on Si surfaces.<sup>11</sup> A small amount of deposited Cu on SiO<sub>2</sub> at a high temperature can form Cu<sub>3</sub>Si, which acts as a catalytic element and enhances the decomposition of SiO<sub>2</sub> into SiO at the SiO<sub>2</sub>/Si interface (Si + SiO<sub>2</sub> → SiO).<sup>11,63,64</sup> This further promotes the formation of voids at the interface.<sup>11</sup> Initially, the voids formed can have different shapes, which may eventually grow to the morphology that is matching with the substrate symmetry. The void structures play an important role in Cu–Si intermixing and can act as a template for the growth of islands.<sup>11</sup> Annealing at 450 °C can initiate the intermixing of Cu and Si and can facilitate the formation of silicide nanocrystallites following the substrate symmetry<sup>65</sup> through a void-filling mechanism in the presence of a native SiO<sub>2</sub> barrier of 4 nm.<sup>34</sup>

SEM investigations performed on the grown sample further validate the triangular morphology of the nanoislands (Figure 2a,b) and the formation of half-filled voids (Figure 2c, marked in a circle) on the sample surface. The lateral dimension of the triangular islands in the SEM images is around 150 nm. We also see direct evidence of spherical, partially, and fully formed triangular islands on the surface, which are marked in single,

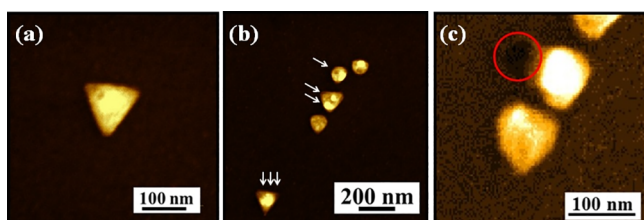


**Figure 2.** SEM micrographs of the nanoislands formed on the SiO<sub>2</sub>/Si (111) surface. (a) Evidence of an individual triangular island. (b) Array of spherical (marked in single arrow), partially formed triangular (marked in double arrow), and fully formed triangular (marked in triple arrow) islands on SiO<sub>2</sub>/Si (111) substrate. (c) A half-filled void is shown (marked in red circle).

double, and triple arrows, respectively, in Figure 2b. On an oxidized surface, because of its much lower surface free energy, the growth of nearly spherical islands is expected.<sup>66</sup> The spherical or nearly spherical islands (Figure 2b,c) observed in the SEM micrographs are indeed smaller in dimension with a diameter less than 100 nm compared to the triangular islands with side lengths around 150 nm or above (Figure 2b,c). A smaller dimension of the spherical islands compared to the triangular ones and signature of partially grown triangular islands in the SEM images (Figure 2b,c) are the direct manifestation of the evolution of islands from spherical to a triangular shape. Evidence of half-filled voids seen in AFM (Figure 1c,d) and SEM investigations (Figure 2c, marked with circle) is a clear demonstration of the faster growth of the voids than that of the nanocrystallites. From all these analyses of AFM and SEM studies, it is well evident that the growth of islands is taking place via a void-filling mechanism.<sup>11</sup> At the initial stage of growth, Cu–Si precipitates at the voids, giving rise to small spherical islands due to a comparatively less surface energy of SiO<sub>2</sub> than Si. These spherical islands eventually grow as triangular nanocrystallites following the three-fold crystal symmetry of the substrate as well as that of Cu to minimize the system energy through shape transformation.<sup>11</sup> However, the formation of voids, diffusion of Cu, and evolution of nanocrystallites will all be limited by the amount of deposited Cu, growth and annealing temperature, duration of annealing, and thickness of the SiO<sub>2</sub> layer. In our case, even on a thick oxide layer of 270 nm, we observe the formation of triangular voids following the substrate crystal symmetry and growth of triangular nanocrystallites through a void-filling mechanism, which provides crucial insight related to fundamental studies on growth, a hitherto unreported observation for material growth on a substantially thick dielectric.

**3.2. XPS Studies.** XPS studies were carried out to examine the elemental composition of the sample. Figure 3a is the

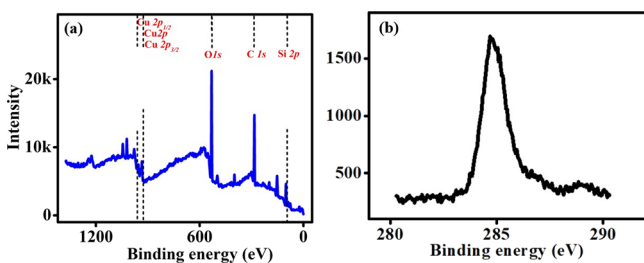


**Figure 3.** (a) XPS survey scan. (b) C 1s calibration peak.

survey scan of the sample obtained using Al K $\alpha$  beam, whereas Figure 3b is the high-resolution C 1s line. Figure 4 shows the

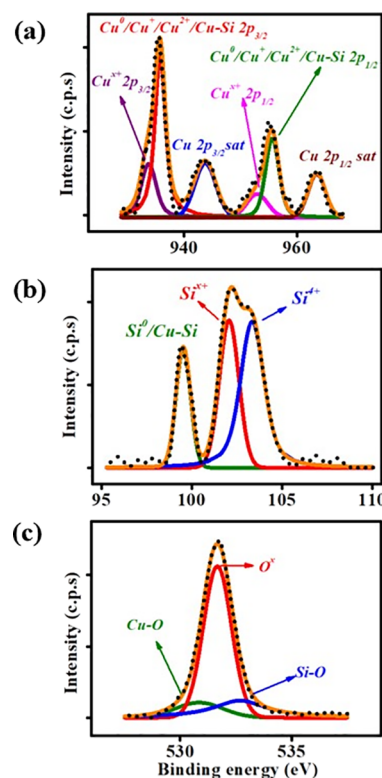


**Figure 4.** High-resolution XPS spectra of the grown film. (a) Cu 2p, (b) Si 2p, and (c) O 1s core level data along with the fittings are shown.

XPS measurements carried out on the grown film. High-resolution Cu 2p (Figure 4a), Si 2p (Figure 4b), and O 1s (Figure 4c) peaks in the XPS studies reveal various chemical compositions of the film. The deconvolution of the Cu 2p spectrum is shown in Figure 4a. The peak centered at 932.9 eV is assigned to a Cu<sup>x+</sup> oxidation state that can be related to the formation of an additional mixed state of Cu–O–Si.<sup>31</sup> The peak at 934.9 eV in Figure 4a is assigned to Cu 2p<sub>3/2</sub> with contributions that may come from oxide phases of Cu in +1 and +2 oxidation states,<sup>56,63,67</sup> metallic Cu, and Cu silicide. The binding energies of metallic Cu, silicide phase, and the oxide states (Cu<sub>2</sub>O, CuO)<sup>31,68</sup> are reported to be very close to each other.<sup>56,63</sup> As a result, it is usually difficult to resolve individual signature in the XPS spectrum.<sup>69,70</sup> Also, evidence of prominent satellite peaks in the Cu 2p spectrum is a clear indication that the sample mainly contains a CuO phase.<sup>69,70</sup> The peak at binding energy 942.9 eV is associated with the Cu 2p<sub>3/2</sub> satellite peak.<sup>67</sup> The band at 952.2 eV is attributed to the Cu<sup>x+</sup> state in Cu 2p<sub>1/2</sub>, and the peak at 954.8 eV is associated with Cu 2p<sub>1/2</sub> from different chemical states of Cu mostly and CuO.<sup>67</sup> The last peak observed at 962.7 eV in the Cu 2p spectrum is the Cu 2p<sub>1/2</sub> satellite peak.<sup>67,71,72</sup> It is important to highlight that the spontaneous oxidation of Cu surfaces with air is also a possibility since samples were exposed to ambient air before XPS analysis. The peaks corresponding to the Cu 2p band in Figure 4a are relatively broad with FWHM falling in the range between 2.3 and 4.4 eV that further corroborates the formation of different Cu–oxide and Cu–silicide phases in the sample.<sup>56</sup>

The XPS spectrum from the Si 2p band and the fitted curves are shown in Figure 4b. In the fitted spectra, the peak at 98.7 eV is assigned to elemental Si<sup>73</sup> or the formation of a silicide phase in the sample.<sup>56,63</sup> The peak centered at 101.3 eV is attributed to the Si<sup>x+</sup> states, the presence of which might be due to the formation of the additional state of Cu–O–Si after the deposition of Cu.<sup>31</sup> The peak at 102.6 eV corresponds to the Si<sup>4+</sup> state in the SiO<sub>2</sub> layer.<sup>31</sup> The 1.55 eV of FWHM of this peak could be associated with the Cu/SiO<sub>2</sub> interface formation.<sup>31</sup> The binding energy of the Si 2p band in the SiO<sub>2</sub> matrix can vary by 1.5 eV depending on the coordination number, oxidation states, and chemical compositions during interface formation.<sup>31</sup> Therefore, the 102.6 eV feature, which is the signature of Si 2p peak in the SiO<sub>2</sub> layer, could be associated with the modification of the chemical environment and subsequent formation of the interface after Cu deposition.<sup>31</sup>

High-resolution O 1s peak and corresponding fitting of the data are shown in Figure 4c. Results obtained from the fit to O 1s peak further substantiate the results obtained from Cu 2p (Figure 4a) and Si 2p (Figure 4b) high-resolution XPS spectra. In the fitted data, the first peak position centered at 530.8 eV is due to the formation of copper oxides, mostly CuO,<sup>31,74</sup> in the film. The peak centered at 531.7 eV represents an O<sup>x</sup> state, which could be due to the formation of a mixed oxide state related to Cu–O–Si in the sample.<sup>31,75</sup> The peak at 532.7 eV is coming from O in SiO<sub>2</sub> matrix,<sup>31,75</sup> which is also observed as a 102.6 eV peak in the Si 2p spectrum in a Si<sup>4+</sup> state. Details of the deconvolution parameters are given in Table 1.<sup>61</sup>

**Table 1. Fitting Parameters of the High-Resolution XPS Spectra of Cu 2p, Si 2p, and O 1s**

spectra	composition	peak position	FWHM	std. deviation
Cu 2p	Cu <sup>x+</sup> 2p <sub>3/2</sub>	932.9	3.16	
	Cu(0)/Cu <sup>+</sup> /Cu <sup>2+</sup> /Cu–Si 2p <sub>3/2</sub>	934.9	2.3	0.07
	Cu 2p <sub>3/2</sub> sat	942.9	4.4	0.15
	Cu <sup>x+</sup> 2p <sub>1/2</sub>	952.2	4.34	
	Cu(0)/Cu <sup>+</sup> /Cu <sup>2+</sup> /Cu–Si 2p <sub>1/2</sub>	954.8	2.8	0.14
Si 2p	Cu 2p <sub>1/2</sub> sat	962.7	3.6	0.24
	Si(0)/Cu–Si	98.7	0.95	0.01
	Si <sup>x+</sup>	101.3	1.27	0.10
O 1s	Si <sup>4+</sup>	102.6	1.55	0.14
	Cu–O	530.8	2.5	0.47
	O <sup>x+</sup>	531.7	1.5	0.03
	Si–O	532.7	2.8	0.2

Subsequent approximations carried out to the high-resolution Cu 2p, Si 2p, and O 1s XPS spectra were helpful to quantify various chemical and structural phases that were formed at the interface after the deposition of Cu. The formation of copper oxide states (mostly Cu<sup>2+</sup>) is obvious from the peaks centering at 934.9, 942.9, 954.8, and 962.7 eV in the Cu 2p (Figure 4a) and the peak at 530.8 eV in the O 1s spectra. Interestingly, we observed the emergence of a mixed Cu–O–Si phase, which is apparent from the peaks centering at 932.9 and 952.2 eV in the Cu 2p, 101.3 eV in the Si 2p, and at 531.7 eV in the O 1s spectra. The results are consistent and could be validated by considering mainly three simultaneous interface processes: first, mixing of Cu and O to form the oxides; second, the formation of the Cu–O–Si mixed-phase;

and third, mixing of Cu and silicon to form the Cu-silicide phase. We have calculated the concentration of each compound phase formed in the film by considering the percentage peak area under the fitted curves. A qualitative estimation of the concentration of each phase formed in the film is shown in Table 2. As we can see, the concentration of the mixed additional phase is the highest with ~41% in the film followed by Cu oxides and Si oxide, which are around 37 and 22% respectively.

**Table 2. Percentage Concentration of Various Chemical Phases Present in the Sample**

spectrum	phase	composition (%)
Cu 2p	Cu(0)/Cu <sup>+</sup> /Cu <sup>2+</sup> /Cu–Si	80
	Cu–O–Si	20
Si 2p	Si(0)/Cu–Si	20
	Cu–O–Si	33
	Si–O	47
O 1s	Cu–O	12
	Cu–O–Si	70
	Si–O	18
total composition (%)	Cu(0)/Cu <sup>+</sup> /Cu <sup>2+</sup> + Cu–Si	37
	Cu–O–Si	41
	Si–O	22

When metallic copper is evaporated onto SiO<sub>2</sub>/Si(111) at an elevated temperature and subsequently annealed, Cu diffuses into the substrate. However, the diffusion and intermixing of Cu and Si are limited by the presence of the SiO<sub>2</sub> layer and temperature.<sup>1</sup> In our case, we have a 270 nm-thick oxide over Si(111) as the substrate. The diffusivity of Cu in intrinsic Si is reported to be almost two orders of magnitude greater than that in SiO<sub>2</sub>.<sup>76,77</sup> Thus, the SiO<sub>2</sub> layer acts as a barrier for Cu diffusion, promoting the oxidation of Cu over the formation of Cu silicide. The two main reasons for the interface mixing of Cu and Si are the solid-state chemical reactions at the interface at an elevated temperature and the increase in diffusivity of Cu atoms in the Si matrix compared to the SiO<sub>2</sub> layer. The diffusivity of Cu in intrinsic Si is reported to be  $(3.03 \pm 0.3) \times 10^{-4} e^{(-0.18 \pm 0.01) \text{ eV}/k_B T} \text{ cm}^{-2}/\text{s}$ , and in SiO<sub>2</sub>, it is  $7.6 \times 10^{-6} e^{-1.82 \text{ eV}/k_B T} \text{ cm}^{-2}/\text{s}$ .<sup>11</sup> However, the diffusion of Cu into Si increases by an order of magnitude as the temperature is raised from RT to above 120 °C.<sup>42</sup> When Cu atoms diffuse through the SiO<sub>2</sub> layer, it can combine with oxygen to form oxides. The kinetics of oxidation depends on various factors like temperature, annealing time, etc. Even at a lower temperature of ~150 °C, Cu is reported to form oxides with Cu atoms in the +1 oxidation state.<sup>78</sup> In general, we can get a mixed oxide phase with Cu in +1 and +2 oxidation states at a temperature around 600 °C and a pure CuO (Cu in the +2 state) at around 1000 °C.<sup>78</sup> Therefore, we expect the formation of Cu oxide in both +1 and +2 oxidation states with higher concentration than silicides due to a thick SiO<sub>2</sub> layer, which interacts with Cu vapors to form oxides and the mixed chemical state involving Cu–O–Si bonds, thus limiting the interaction of Cu and Si. Benito and Flores<sup>31</sup> have studied the formation of Cu oxide states, mixed chemical states (Cu–O–Si), and silicide phases w.r.t. the Cu/Si ratio. According to their results, the mixed chemical state of Cu–O–Si is formed for the lowest Cu/Si ratio with the highest concentration. In our case, only around 60 Å Cu was deposited and as a result, it is quite likely that we get to see a substantial portion of the film (~41%) containing

an intermediate mixed chemical state in the XPS data. It was proposed that the oxygen from the SiO<sub>2</sub> substrate initially reacts with Cu and forms a thin layer of Cu oxides and Cu–O–Si phase. In the Cu–SiO<sub>2</sub>/Si interface, Cu<sup>x+</sup> in Cu 2p<sub>3/2</sub> should form at a binding energy lower than that of Cu<sup>2+</sup>, O<sup>x-</sup> should form in O 1s in between the binding energies of Cu–O and Si–O, and Si<sup>x+</sup> in Si 2p should form at a binding energy below that of SiO<sub>2</sub>, giving rise to an intermediate state of Cu–O–Si.<sup>31</sup> The migration of Si atoms toward the surface is also an important phenomenon to form this intermediate state.<sup>31,75</sup>

Using eq 1, we have calculated the individual atomic concentration within the Cu–O–Si phase. The highest concentration is observed for oxygen, ~86% followed by Si and Cu, at ~13 and ~1%, respectively.

The growth of Cu silicide in the Cu–SiO<sub>2</sub>/Si system is mainly governed by the thickness of the SiO<sub>2</sub> barrier and the temperature, which would decide about the diffusion of Cu into Si to form Cu silicide. Voids present on the surface also play an important role to accelerate the formation of the silicide phase. The enthalpy of mixing of Cu and Si is almost the same at RT because of the similarity in their crystal structure. Thus, the intermixing is not energetically favorable in such conditions.<sup>79</sup> Copper-rich silicides (Cu<sub>4</sub>Si, Cu<sub>3</sub>Si) can be formed by the reaction between copper layers and silicon substrates covered by a thin silicon oxide layer of 2–4 nm during heat treatment in the temperature range of 600–750 °C.<sup>11,38</sup> The enthalpy of formation of the most stable Cu silicide (Cu<sub>3</sub>Si) has been calculated to be –24.4 kJ/mol<sup>79</sup> at RT. The catalytic action of Cu silicide further helps in breaking Si–Si and Si–O bonds (which would otherwise occur at higher temperature), thereby enhancing the formation of voids and more silicide formation. These extra silicides will then generate additional defects at the SiO<sub>2</sub>/Si interface promoting the growth of more islands.<sup>65</sup> We expect the formation of Cu-silicide due to the migration of Cu mainly through the voids or defects on the surface. As a result, Cu-silicide might be the main compound phase of the sparsely distributed islands with an overall lower concentration in the film due to low number density of the islands on the surface. This will make it difficult to be detected and resolved by the XPS.

**3.3. Raman Spectroscopy.** Raman spectroscopy studies are shown in Figure 5. Figure 5a exhibits the Raman transitions from a SiO<sub>2</sub>/Si substrate. The most intense Raman shift observed at 518 cm<sup>-1</sup> is attributed to main one-phonon (optical) peak of Si,<sup>80</sup> whereas a relatively less intense broad band with a doublet feature observed between 900 and 1000 cm<sup>-1</sup> with peaks centering at 940 and 969 cm<sup>-1</sup> (inset, Figure 5a), respectively, is associated to two phonon overtones related to the transverse optical branch of Si.<sup>80</sup> We could resolve all the fine structures between 200 and 450 cm<sup>-1</sup> of Si,<sup>54,80–82</sup> by performing a multi Gaussian peak fit to the experimental data (Figure 5c). Peaks at 246, 298, 359, and 428 cm<sup>-1</sup> (Figure 5c) in the fitted data correspond to optical phonons.<sup>54,80–82</sup> Raman shifts from the Cu-deposited film (Figure 5b) are somewhat displaced compared to the features observed on the bare SiO<sub>2</sub>/Si substrate along with the signature of additional peaks/onsets in the spectrum. Cu with an FCC crystal structure does not have any Raman active mode. We observe peak features from the grown film (Figure 5b,d) at wavenumbers 138, 249, 301, 320, 424, 469, 518, 607, 943, and 980 cm<sup>-1</sup>, which could be associated with various vibrational modes ascribed to the film and the substrate. The convoluted peak feature in the range of 200 to 450 cm<sup>-1</sup> of the deposited

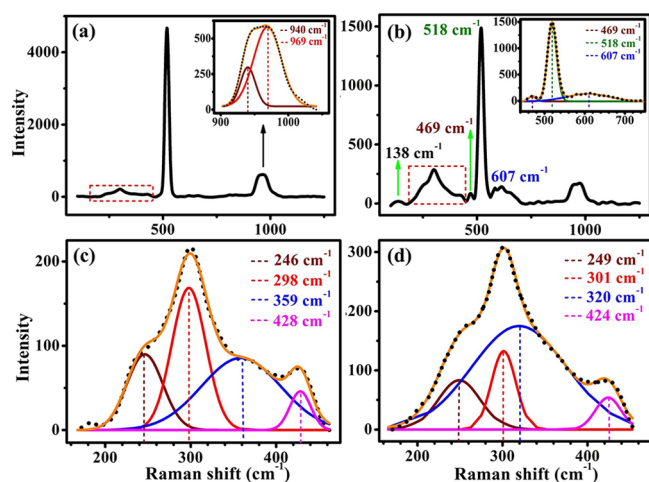


**Figure 5.** (a, b) Raman spectra of SiO<sub>2</sub>/Si before (a) and after Cu deposition (b). The regions from 200 to 450 cm<sup>-1</sup> marked in red dashed rectangles in (a, b) are shown in (c, d).

film was deconvoluted in a similar fitting process considering various Gaussian peaks discussed above. The formation of Cu<sub>2</sub>O in the system is validated by the presence of the onset at 138 cm<sup>-1</sup>.<sup>83</sup> Raman shifts related to CuO should be seen at 297 and 626 cm<sup>-1</sup>,<sup>83</sup> whereas the formation of the Cu–O–Cu<sub>2</sub>O mixed phase is reported to exhibit a broad feature peaking at 630 cm<sup>-1</sup>.<sup>83</sup> In our fitted data (Figure 5d), we observed an onset at 301 and a broad feature centering at 607 cm<sup>-1</sup> (Figure 5b). The feature at 301 cm<sup>-1</sup> could well be correlated with the formation of the CuO phase,<sup>83</sup> whereas a large downshift of 23 cm<sup>-1</sup> of the 607 cm<sup>-1</sup> peak compared to the reported value of 630 cm<sup>-1</sup><sup>83</sup> might as well be associated with the formation of the Cu–O–Si intermediate phase in the sample. The peak feature observed at 469 cm<sup>-1</sup> (Figure 5b) could be assigned to the emergence of the Cu-silicide phase in the grown film.<sup>84</sup> Fitted data in the range of 200 to 450 cm<sup>-1</sup> for both the substrate and the film (Figure 5c,d) exhibit four peaks related to Si acceptors/donors electronic Raman transitions<sup>54</sup> among which the 428 cm<sup>-1</sup> peak from the substrate could also be due to symmetrical Si–O–Si stretching modes principally involving the motion of oxygen atoms of the SiO<sub>2</sub>/Si substrate.<sup>85</sup> Features related to Cu oxidation are supposed to appear within ~630 cm<sup>-1</sup>. We see a shift in peak positions and a change in intensity in the fitted Raman transitions (Figure 5d) (200–450 cm<sup>-1</sup>) of the grown film compared to the substrate (Figure 5c). A clear shift observed in the peak features in this region requires further studies to discuss. From the Raman studies discussed here, evidence of the formation of Cu-oxides and Cu-silicide is established; however, it is difficult to comment certainly on the Raman active signatures of the Cu–O–Si phase as there is hardly any theoretical or experimental studies available so far related to this. We believe that our results associated with well-defined Raman shifts in the characteristic peak features might provide important insight toward future investigations to develop a quantitative understanding of the Raman transitions of the intermediate Cu–O–Si phase.

**3.4. Electrical Characterizations.** We have carried out two probe transport studies and RT Hall measurements following vdP geometry on our sample. Schematics of the electrical characterizations are shown in Figure 6. The results obtained from two electrode measurements are shown in

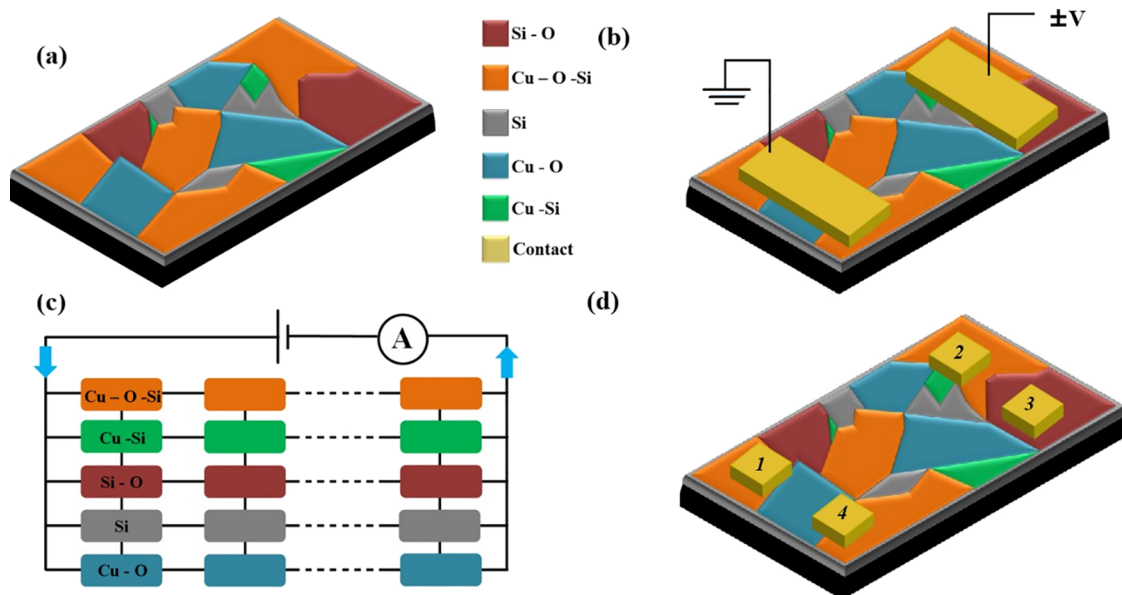


**Figure 6.** Schematic representation of electrical transport studies of Cu film grown on SiO<sub>2</sub>/Si with various compound phases. (a) Domains of different phases are shown on the surface in different colors. (b) Schematic depiction of two probe electrode measurements and (c) a probable model of the two-electrode current conduction through the complex film network. (d) Schematic of the vdP geometry.

Figure 7, and the data procured from Hall investigations are given in Table 3. Gold electrodes (140 nm thick) were made

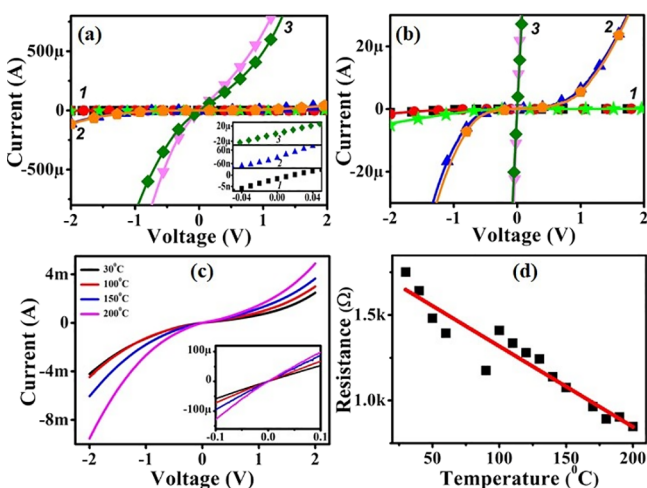


**Figure 7.** Two probe electrical measurements performed on the Cu-grown film. (a) RT  $I$ - $V$  characteristics exhibiting various conducting channels (denoted as 1, 2, and 3 in the plot) in the film. The ohmic nature of the contacts around 0 V is shown as an inset in (a). (b) Rectified current scale data of (a) keeping the same  $x$  scale to show further the three different current paths, which were observed within the same Cu-grown sample. (c) Temperature-dependent  $I$ - $V$  characteristics from 30 to 200 °C along the current path 3. Inset of (c) displays the ohmic nature of the contacts. (d) Resistance vs temperature plot for path 3

**Table 3.** Hall Measurement Data

carrier concentration, $p_s$ ( $\text{cm}^{-2}$ )	Hall mobility, $\mu$ ( $\text{cm}^2 \text{V}^{-1} \text{s}^{-1}$ )	sheet resistance, $R_s$ ( $\Omega$ )
$4.93 \times 10^{10}$	34.24	$3.7 \times 10^6$

on the sample surface using a thermal evaporation system, and the current–voltage ( $I$ - $V$ ) spectra were acquired across the electrodes from RT to 200 °C. Figure 6a shows the RT  $I$ - $V$  spectra obtained for a voltage range of  $-2$  to  $+2$  V along different current paths. The set of curves denoted as 1 in Figure 7a exhibit resistance of the order of  $10^3 \Omega$ , whereas the curves 2 and 3 (Figure 7a) show resistance of the order of  $10^5$  and  $10^7 \Omega$  respectively. The ohmic nature of the contacts around zero bias is shown as an inset in Figure 7a. Figure 7b is the rectified current scale data of Figure 7a to clearly emphasize further on different current channels that exist in the film. Figure 7c exhibits  $I$ - $V$  measurements from 30 to 200 °C obtained along a particular path without disturbing the probe positions. This set of data reveals a resistance range, which is similar to that of 1 in Figure 7a,b. The slope of the  $I$ - $V$  curves (Figure 7c) increases with an increase in temperature exhibiting the highest slope at 200 °C, indicating the lowest resistance of the sample at this temperature. A signature of non-linearity, which is evident in the data set in Figure 7c, is presumably arising from the difference in Schottky barrier heights of the Cu species and the Au contacts. We have calculated the resistance values for each temperature from the corresponding  $I$ - $V$  spectrum and plotted the values as a function of temperature. A linear fit to the resistance vs temperature plot (Figure 7d) shows a negative slope revealing a semiconducting nature of the channel.

Two electrode  $I$ - $V$  measurements performed at various probe positions across the film disclose varying electrical nature (Figure 7a,b), which must be due to the domains of different Cu-induced phases in the film. As a result, the  $I$ - $V$  spectra obtained along particular lines may not be sufficient to comment about the overall electrical behavior, especially for a complex film network like the one discussed here. Therefore, we further carried out RT Hall measurements on the sample following vdP geometry. Table 3 summarizes the results obtained from Hall studies. Hall measurements reveal an n-type carrier density ( $n_s$ ) of  $4.93 \times 10^{10} \text{ cm}^{-2}$  of the Cu-deposited film. The overall sheet resistance ( $R_s$ ) of the film is

$3.7 \times 10^6 \Omega$ , and the carrier mobility ( $\mu$ ) is  $34.24 \text{ cm}^2 \text{ V}^{-1} \text{ s}^{-1}$ . The thickness of the grown film, as we have seen from AFM and SEM investigations, is not uniform with evidence of sparsely distributed islands, voids, and partially filled voids on the sample surface. This makes the resistivity measurement and quantitative estimation further difficult. However, the resistances calculated from the  $I$ - $V$  curves corresponding to different channels lie within  $10^3$  to  $10^7 \Omega$ , which is typically the resistance range exhibited by the semiconducting materials. A temperature-dependent resistance measurement (Figure 7c) across a particular channel (current path 3) also shows a decrease in resistance with an increase in temperature corroborating further about the channel being semiconducting. Hall studies again provide the average sheet resistance of the film, which is of the order of  $10^6 \Omega$  and n-type.

The additional phase of Cu-O-Si and the Cu oxides ( $\text{Cu}_2\text{O}$  + CuO) constitute together a substantial amount ( $\sim 78\%$ ) of the film, whereas the silicide phase is present in a small amount. Experiments performed based on electrical current measurements on metal silicides exhibit either metallic or semiconducting behavior.<sup>11,86,87</sup> Cu silicides usually come under metallic silicides.<sup>11</sup> Cu oxides (both in +1 and +2 states), on the other hand, are p-type semiconductors with an energy band gap of 2.1 eV for  $\text{Cu}_2\text{O}$  and 1.21–1.51 eV for CuO.<sup>78</sup> However, very little is known about the electrical characteristics of the Cu-O-Si phase. The RT resistivity of Cu is in the range of  $0.01$ – $1 \Omega \text{ cm}$ ,  $\text{Cu}_2\text{O}$  is in the range of  $10^3$  to  $10^8 \Omega \text{ cm}$ , and  $\text{Cu}_3\text{Si}$  is in the range of  $55$ – $60 \mu\Omega \text{ cm}$ , whereas intrinsic Si has a resistivity of the order of  $10^5 \Omega \text{ cm}$ . We attribute the semiconducting behavior of the film due to the coexistence of Cu-O-Si and Cu oxides. All Cu oxides (CuO and  $\text{Cu}_2\text{O}$ ) are p-type semiconducting. The Cu-O-Si mixed phase has unknown electrical properties. The film contains  $\sim 41\%$  of the mixed phase. The overall electrical properties of the film should be dominated by the main phases formed. Since we see an n-type semiconducting behavior with an average film resistance of the order of  $10^6 \Omega$ , it means that the mixed-phase cannot be metallic but mostly semiconducting only. This also indicates that the amount of Cu-silicides is less and mostly scattered throughout the film. Thus, the current could not find any metallic paths.

#### 4. CONCLUSIONS

The growth of Cu at  $600^\circ\text{C}$  on a 270 nm-thick  $\text{SiO}_2$  layer on a Si(111) substrate has been investigated. Upon deposition, Cu grows as sparsely distributed triangular islands, while the morphology of the Cu-grown film is continuous (in the AFM and SEM images) with the presence of different domains of different elemental compositions. The growth of triangular islands occurs via a void-filling mechanism through diffusion and segregation where a three-fold crystal symmetry of the Cu as well as that of the substrate gets reflected on the morphology of the islands. AFM studies also clearly indicate empty and half-filled triangular voids on the surface, a case of direct manifestation of faster growth of voids than islands. These results provide valuable insight of Cu growth at an elevated temperature on the Si substrate that is covered with a considerably thick (270 nm) thermally grown  $\text{SiO}_2$  dielectric. XPS measurements reveal the emergence of an intermediate Cu-O-Si phase in the grown film with atomic concentrations of  $\sim 1$ ,  $\sim 86$ , and  $\sim 13\%$  for Cu, O, and Si, respectively. This intermediate state, as high as  $\sim 41\%$ , dominates the film composition followed by Cu oxides ( $\sim 37\%$ ) and Si oxides

( $\sim 22\%$ ). The formation of all these phases can be associated with the temperature of annealing, thickness of the  $\text{SiO}_2$  barrier, amount of the deposited Cu, diffusion and reactivity of Cu in the  $\text{SiO}_2/\text{Si}$  system, and migration of Si toward the surface. Two probe electrical measurements carried out on the Cu-grown film exhibit different current channels across the film with resistance varying from  $10^3$  to  $10^7 \Omega$  indicating evidence of different phase domains that exist in the film. Hall measurements performed using vdP geometry confirm an n-type semiconducting nature of the grown film with an overall sheet resistance of the order of  $10^6 \Omega$ .

#### AUTHOR INFORMATION

##### Corresponding Author

**Kuntala Bhattacharjee** – Institute of Physics, Bhubaneswar, Odisha 751005, India; Department of Space, Indian Institute of Space Science and Technology, Thiruvananthapuram, Kerala 695 547, India; [orcid.org/0000-0002-7977-1961](https://orcid.org/0000-0002-7977-1961); Email: [kbhattacharjee@iopb.res.in](mailto:kbhattacharjee@iopb.res.in), [kuntala.iopb@gmail.com](mailto:kuntala.iopb@gmail.com); Fax: +91-674-2300142

##### Authors

**Reshmi Sreedharan** – Institute of Physics, Bhubaneswar, Odisha 751005, India; Department of Space, Indian Institute of Space Science and Technology, Thiruvananthapuram, Kerala 695 547, India

**Manu Mohan** – Department of Space, Indian Institute of Space Science and Technology, Thiruvananthapuram, Kerala 695 547, India

**Sonia Saini** – Department of Space, Indian Institute of Space Science and Technology, Thiruvananthapuram, Kerala 695 547, India; Laboratory for Electro-Optics Systems (LEOS), ISRO, Bengaluru 560057, India

**Anupam Roy** – Microelectronics Research Center, The University of Texas at Austin, Austin, Texas 787 758, United States; [orcid.org/0000-0003-1207-0981](https://orcid.org/0000-0003-1207-0981)

Complete contact information is available at:  
<https://pubs.acs.org/10.1021/acsoomega.1c02646>

##### Notes

The authors declare no competing financial interest.

#### ACKNOWLEDGMENTS

The authors sincerely thank Dr. Hema C P Movva for fruitful discussion. K.B. is particularly thankful to the DST Mobility Scheme for providing her with the infrastructure, funding, and professional and personal stability to carry out this work.

#### REFERENCES

- (1) Sekar, K.; Satyam, P. V.; Kuri, G.; Mahapatra, D. P.; Dev, B. N. An RBS Study of Interdiffusion across a Brominated Si(111)/Cu Interface with and without a Barrier Layer. *Nucl. Instrum. Methods Phys. Res., Sect. B* **1993**, *73*, 63–70.
- (2) Roy, A.; Sundaravel, B.; Batabyal, R.; Dev, B. N. Fractal Pattern Formation in Thermal Grooving at Grain Boundaries in Ag Films on Si(111) Surfaces. *Thin Solid Films* **2012**, *520*, 5086–5090.
- (3) Sundaravel, B.; Das, A. K.; Ghose, S. K.; Sekar, K.; Dev, B. N. Epitaxial Growth of Silver on Br-Passivated Si(111) Substrates under High Vacuum. *Appl. Surf. Sci.* **1999**, *137*, 11–19.
- (4) Sundaravel, B.; Das, A. K.; Ghose, S. K.; Rout, B.; Dev, B. N. Improvement of Ag(1 1 1) Epitaxy on Si(1 1 1) by MeV  $\text{Si}^+$  Irradiation and Ion Microbeam Analysis of Thermally Induced Morphology. *Nucl. Instrum. Methods Phys. Res., Sect. B* **1999**, *156*, 130–134.

- (5) Sundaravel, B.; Sekar, K.; Kuri, G.; Satyam, P. V.; Dev, B. N.; Bera, S.; Narasimhan, S. V.; Chakraborty, P.; Caccavale, F. XPS and SIMS analysis of gold silicide grown on a bromine passivated Si(111) substrate. *Appl. Surf. Sci.* **1999**, *137*, 103–112.
- (6) Sekar, K.; Kuri, G.; Satyam, P. V.; Sundaravel, B.; Mahapatra, D. P.; Dev, B. N. Shape Transition in the Epitaxial Growth of Gold Silicide in Au Thin Films on Si(111). *Phys. Rev. B* **1995**, *51*, 14330–14336.
- (7) Sumitomo, K.; Kobayashi, T.; Shoji, F.; Oura, K.; Katayama, I. Hydrogen-Mediated Epitaxy of Ag on Si(111) as Studied by Low-Energy Ion Scattering. *Phys. Rev. Lett.* **1991**, *66*, 1193–1196.
- (8) Nishiyama, A.; Ter Horst, G.; Zagwijn, P. M.; van Den Hoven, G. N.; Frenken, J. W. M.; Garten, F.; Schlatmann, A. R.; Vrijmoeth, J. Growth Mode and Interface Structure of Ag on the HF-Treated Si(111):H Surface. *Surf. Sci.* **1996**, *350*, 229–238.
- (9) Pavlenko, V. I.; Cherkashina, N. I.; Zaitsev, S. V. Fabrication and Characterization of Nanocomposite Films Al, Cu/Al and Cr/Al Formed on Polyimide Substrate. *Acta Astronaut.* **2019**, *160*, 489–498.
- (10) Schlesinger, M. E. Thermodynamics of Solid Transition-Metal Silicides. *Chem. Rev.* **1990**, *90*, 607–628.
- (11) Li, S.; Cai, H.; Gan, C. L.; Guo, J.; Dong, Z.; Ma, J. Controlled Synthesis of Copper-Silicide Nanostructures. *Cryst. Growth Des.* **2010**, *10*, 2983–2989.
- (12) Park, J.-H.; Han, D.-S.; Kang, Y.-J.; Shin, S.-R.; Park, J.-W. Self-Forming Al Oxide Barrier for Nanoscale Cu Interconnects Created by Hybrid Atomic Layer Deposition of Cu–Al Alloy. *J. Vac. Sci. Technol., A* **2014**, *32*, No. 01A131.
- (13) Lambert, S.; Cellier, C.; Grange, P.; Pirard, J.-P.; Heinrichs, B. Synthesis of Pd/SiO<sub>2</sub>, Ag/SiO<sub>2</sub>, and Cu/SiO<sub>2</sub> Cogelled Xerogel Catalysts: Study of Metal Dispersion and Catalytic Activity. *J. Catal.* **2004**, *221*, 335–346.
- (14) Janas, J.; Gurgul, J.; Socha, R. P.; Dzwigaj, S. Effect of Cu Content on the Catalytic Activity of CuSiBEA Zeolite in the SCR of NO by Ethanol: Nature of the Copper Species. *Appl. Catal., B* **2009**, *91*, 217–224.
- (15) van den Oetelaar, L. C. A.; Partridge, A.; Stapel, P. J. A.; Flipse, C. F. J.; Brongersma, H. H. A Surface Science Study of Model Catalysts. 1. Quantitative Surface Analysis of Wet-Chemically Prepared Cu/SiO<sub>2</sub> Model Catalysts. *J. Phys. Chem. B* **1998**, *102*, 9532–9540.
- (16) van den Oetelaar, L. C. A.; Partridge, A.; Toussaint, S. L. G.; Flipse, C. F. J.; Brongersma, H. H. A Surface Science Study of Model Catalysts. 2. Metal–Support Interactions in Cu/SiO<sub>2</sub> Model Catalysts. *J. Phys. Chem. B* **1998**, *102*, 9541–9549.
- (17) Parajuli, O.; Kumar, N.; Kipp, D.; Hahm, J. Carbon Nanotube Cantilevers on Self-Aligned Copper Silicide Nanobeams. *Appl. Phys. Lett.* **2007**, *90*, 173107.
- (18) Bawaked, S.; Narasimharao, K. Structural and Catalytic Properties of Copper Silicate Nanomaterials. *Sci. Rep.* **2020**, *10*, 518.
- (19) Anbarasan, R.; Palanikumar, S.; Devi, A. A.; Chen, P.-H.; Tung, K. L. Characterization and Application of Cu Based Superhydrophobic Catalyst. *Prog. Nat. Sci. Mater. Int.* **2019**, *29*, 371–378.
- (20) Xu, C.; Chen, G.; Zhao, Y.; Liu, P.; Duan, X.; Gu, L.; Fu, G.; Yuan, Y.; Zheng, N. Interfacing with Silica Boosts the Catalysis of Copper. *Nat. Commun.* **2018**, *9*, 3367.
- (21) Ye, R.-P.; Lin, L.; Li, Q.; Zhou, Z.; Wang, T.; Russell, C. K.; Adidharma, H.; Xu, Z.; Yao, Y.-G.; Fan, M. Recent Progress in Improving the Stability of Copper-Based Catalysts for Hydrogenation of Carbon–Oxygen Bonds. *Catal. Sci. Technol.* **2018**, *8*, 3428–3449.
- (22) Liu, Y.; Song, S.; Mao, D.; Ling, H.; Li, M. Diffusion Barrier Performance of Reactively Sputtered Ta–W–N between Cu and Si. *Microelectron. Eng.* **2004**, *75*, 309–315.
- (23) Ahn, H.-J.; Kim, Y.-S.; Kim, W. B.; Sung, Y.-E.; Seong, T.-Y. Formation and Characterization of Cu–Si Nanocomposite Electrodes for Rechargeable Li Batteries. *J. Power Sources* **2006**, *163*, 211–214.
- (24) Shimoi, N.; Tohji, K. Structure and Electrochemical Properties of a Mechanochemically Processed Silicon and Oxide-Based Nanoscale Composite as an Active Material for Lithium-Ion Batteries. *J. Nanotechnol.* **2017**, *2017*, 1–8.
- (25) Mukherjee, R.; Srivastava, P.; Ravindra, P.; Avasthi, S. Doped Cu<sub>2</sub>O/n-Si Heterojunction Solar Cell. In *2018 IEEE 7th World Conference on Photovoltaic Energy Conversion (WCPEC) (A Joint Conference of 45th IEEE PVSC, 28th PVSEC & 34th EU PVSEC)*; IEEE: 2018; pp. 2162–2165, DOI: 10.1109/PVSC.2018.8547485.
- (26) Kumar, V.; Masudy-Panah, S.; Tan, C. C.; Wong, T. K. S.; Chi, D. Z.; Dalapati, G. K. Copper Oxide Based Low Cost Thin Film Solar Cells. In *2013 IEEE 5th International Nanoelectronics Conference (INEC)*; IEEE: 2013; pp. 443–445, DOI: 10.1109/INEC.2013.6466072.
- (27) Mitroi, M. R.; Ninulescu, V.; Fara, L. Tandem Solar Cells Based on Cu<sub>2</sub>O and C-Si Subcells in Parallel Configuration: Numerical Simulation. *Int. J. Photoenergy* **2017**, *2017*, 1–6.
- (28) Liu, Y.; Zhu, J.; Cai, L.; Yao, Z.; Duan, C.; Zhao, Z.; Zhao, C.; Mai, W. Solution-Processed High-Quality Cu<sub>2</sub>O Thin Films as Hole Transport Layers for Pushing the Conversion Efficiency Limit of Cu<sub>2</sub>O/Si Heterojunction Solar Cells. *Sol. RRL* **2020**, *4*, 1900339.
- (29) Kute, A. M.; Waghuley, S. A. Photovoltaic Properties of Nanostructured Copper Sulfide Incorporated Silicon Rich Composites. *J. Mater. Sci.: Mater. Electron.* **2018**, *29*, 16199–16206.
- (30) Aboelfotoh, M. O.; Svensson, B. G. Electrical Properties of Copper-Silicon Schottky Barriers. *Semicond. Sci. Technol.* **1991**, *6*, 647–652.
- (31) Benito, N.; Flores, M. Evidence of Mixed Oxide Formation on the Cu/SiO<sub>2</sub> Interface. *J. Phys. Chem. C* **2017**, *121*, 18771–18778.
- (32) Li, Z.; Tian, Y.; Teng, C.; Cao, H. Recent Advances in Barrier Layer of Cu Interconnects. *Materials* **2020**, *13*, 5049.
- (33) Pavlenko, V. I.; Cherkashina, N. I. Effect of SiO<sub>2</sub> Crystal Structure on the Stability of Polymer Composites Exposed to Vacuum Ultraviolet Radiation. *Acta Astronaut.* **2019**, *155*, 1–9.
- (34) Bo, C.; Yan-hui, J.; Gong-Ping, L.; Xi-Meng, C. Atomic Diffusion in Annealed Cu/SiO<sub>2</sub>/Si (100) System Prepared by Magnetron Sputtering. *Chin. Phys. B* **2010**, *19*, No. 026601.
- (35) Zhang, J.; Liu, C.; Fan, J. Comparison of Cu Thin Films Deposited on Si Substrates with Different Surfaces and Temperatures. *Appl. Surf. Sci.* **2013**, *276*, 417–423.
- (36) Savchenkov, A.; Shukrinov, P.; Mutombo, P.; Slezák, J.; Cháb, V. Initial Stages of Cu/Si Interface Formation. *Surf. Sci.* **2002**, *507–510*, 889–894.
- (37) Shi, J. R.; Lau, S. P.; Sun, Z.; Shi, X.; Tay, B. K.; Tan, H. S. Structural and Electrical Properties of Copper Thin Films Prepared by Filtered Cathodic Vacuum Arc Technique. *Surf. Coat. Technol.* **2004**, *268*, 250–601.
- (38) Benouattas, N.; Mosser, A.; Raiser, D.; Faerber, J.; Bouabellou, A. Behaviour of Copper Atoms in Annealed Cu/SiO<sub>x</sub>/Si Systems. *Appl. Surf. Sci.* **2000**, *153*, 79–84.
- (39) Benouattas, N.; Mosser, A.; Bouabellou, A. Surface morphology and reaction at Cu/Si interface—Effect of native silicon suboxide. *Appl. Surf. Sci.* **2006**, *252*, 7572–7577.
- (40) Zhang, Z.; Wong, L. M.; Ong, H. G.; Wang, X. J.; Wang, J. L.; Wang, S. J.; Chen, H.; Wu, T. Self-Assembled Shape- and Orientation- Controlled Synthesis of Nanoscale Cu<sub>3</sub>Si Triangles, Squares, and Wires. *Nano Lett.* **2008**, *8*, 3205–3210.
- (41) Cemin, F.; Lundin, D.; Furgeaud, C.; Michel, A.; Amiard, G.; Minea, T.; Abadias, G. Epitaxial Growth of Cu(001) Thin Films onto Si(001) Using a Single-Step HiPIMS Process. *Sci. Rep.* **2017**, *7*, 1655.
- (42) Ektessabi, A. M. Temperature Dependence of Atomic Mixing at the Copper-Silicon Interface. *Thin Solid Films* **1993**, *236*, 135–139.
- (43) Dolbak, A. E.; Zhachuk, R. A.; Olshansky, B. Z. Mechanism of Cu Transport along Clean Si Surfaces. *Cent. Eur. J. Phys.* **2003**, *1*, 463–473.
- (44) Zhou, J. B.; Gustafsson, T. Growth of Thin Cu Films on MgO(001). *Surf. Sci.* **1997**, *375*, 221–225.
- (45) Aboelfotoh, M. O.; Krusin-Elbaum, L. Electrical Transport in Thin Films of Copper Silicide. *J. Appl. Phys.* **1991**, *70*, 3382–3384.
- (46) Walter, H.; Roewer, G.; Bohmhammel, K. Mechanism of the Silicide-Catalysed Hydrodehalogenation of Silicon Tetrachloride to Trichlorosilane. *J. Chem. Soc., Faraday Trans.* **1996**, *92*, 4605.

- (47) Selamoglu, N.; Mucha, J. A.; Flamm, D. L.; Ibbotson, D. E. Catalyzed Gaseous Etching of Silicon. *MRS Proc.* **1986**, *75*, 459.
- (48) Kim, I.-C.; Byun, D.; Lee, J. K. Electrochemical Characteristics of Silicon-Metals Coated Graphites for Anode Materials of Lithium Secondary Batteries. *Electrochim. Acta* **2006**, *17*, 661–665.
- (49) Pearson, S. J.; Heo, W. H.; Ivill, M.; Norton, D. P.; Steiner, T. Dilute Magnetic Semiconducting Oxides. *Semicond. Sci. Technol.* **2004**, *19*, R59.
- (50) Ramírez-Ortiz, J.; Ogura, T.; Medina-Valtierra, J.; Acosta-Ortiz, S. E.; Bosch, P.; de Los Reyes, J. A.; Lara, V. H. A Catalytic Application of Cu<sub>2</sub>O and CuO Films Deposited over Fiberglass. *Appl. Surf. Sci.* **2001**, *174*, 177–184.
- (51) Han, K.; Tao, M. Electrochemically Deposited P-n Homojunction Cuprous Oxide Solar Cells. *Sol. Energy Mater. Sol. Cells* **2009**, *93*, 153–157.
- (52) Fernando, C. A. N.; Wethasinghe, S. K. Investigation of Photoelectrochemical Characteristics of N-Type Cu<sub>2</sub>O Films. *Sol. Energy Mater. Sol. Cells* **2000**, *63*, 299–308.
- (53) Koffyberg, F. P.; Benko, F. A. A photoelectrochemical determination of the position of the conduction and valence band edges of p-type CuO. *J. Appl. Phys.* **1982**, *53*, 1173–1177.
- (54) Wright, G. B.; Mooradian, A. Raman Scattering from Donor and Acceptor Impurities in Silicon. *Phys. Rev. Lett.* **1967**, *18*, 608–610.
- (55) Espinós, J. R.; Morales, J.; Barranco, A.; Caballero, A.; Holgado, J. P.; González-Elipe, A. R. Interface Effects for Cu, CuO, and Cu<sub>2</sub>O Deposited on SiO<sub>2</sub> and ZrO<sub>2</sub>. XPS Determination of the Valence State of Copper in Cu/SiO<sub>2</sub> and Cu/ZrO<sub>2</sub> Catalysts. *J. Phys. Chem. B* **2002**, *106*, 6921–6929.
- (56) Sarkar, D. K.; Bera, S.; Narasimhan, S. V.; Chowdhury, S.; Gupta, A.; Nair, K. G. M. GIXRD and XPS Investigation of Silicidation in Ion Beam Mixed Cu/Si(1 1 1) System. *Solid State Commun.* **1998**, *107*, 413–416.
- (57) Yuan, F.-W.; Wang, C.-Y.; Li, G.-A.; Chang, S.-H.; Chu, L.-W.; Chen, L.-J.; Tuan, H.-Y. Solution-Phase Synthesis of Single-Crystal Cu<sub>3</sub>Si Nanowire Arrays on Diverse Substrates with Dual Functions as High-Performance Field Emitters and Efficient Anti-Reflective Layers. *Nanoscale* **2013**, *5*, 9875–9881.
- (58) Horcas, I.; Fernández, R.; Gómez-Rodríguez, J. M.; Colchero, J.; Gómez-Herrero, J.; Baro, A. M. WSXM: a software for scanning probe microscopy and a tool for nanotechnology. *Rev. Sci. Instrum.* **2007**, *78*, No. 013705.
- (59) Roy, A.; Guchhait, S.; Sonde, S.; Dey, R.; Pramanik, T.; Rai, A.; Movva, H. C. P.; Colombo, L.; Banerjee, S. K. Two-Dimensional Weak Anti-Localization in Bi<sub>2</sub>Te<sub>3</sub> thin Film Grown on Si(111)-(7 × 7) Surface by Molecular Beam Epitaxy. *Appl. Phys. Lett.* **2013**, *102*, 163118.
- (60) Chowdhury, S.; Roy, A.; Liu, C.; Alam, M. H.; Ghosh, R.; Chou, H.; Akinwande, D.; Banerjee, S. K. Two-Step Growth of Uniform Monolayer MoS<sub>2</sub> Nanosheets by Metal–Organic Chemical Vapor Deposition. *ACS Omega* **2021**, *6*, 10343–10351.
- (61) Major, G. H.; Fairley, N.; Sherwood, P. M. A.; Linford, M. R.; Terry, J.; Fernandez, V.; Artyushkova, K. Practical Guide for Curve Fitting in X-Ray Photoelectron Spectroscopy. *J. Vac. Sci. Technol., A* **2020**, *38*, No. 061203.
- (62) Fairley, N. *CasaXPS Manual 2.3.15*; Casa Software Limited: 2009.
- (63) Cros, A.; Aboelfotoh, M. O.; Tu, K. N. Formation, Oxidation, Electronic, and Electrical Properties of Copper Silicides. *J. Appl. Phys.* **1990**, *67*, 3328–3336.
- (64) Dallaporta, H.; Liehr, M.; Lewis, J. E. Silicon Dioxide Defects Induced by Metal Impurities. *Phys. Rev. B* **1990**, *41*, 5075–5083.
- (65) Seibt, M.; Griess, G.; Istratov, A. A.; Hedemann, H.; Sattler, A.; Schröter, W. Formation and Properties of Copper Silicide Precipitates in Silicon. *Phys. Status Solidi* **1998**, *166*, 171.
- (66) Roy, A.; Bhattacharjee, K.; Ghatak, J.; Dev, B. N. Growth of epitaxially oriented Ag nanoislands on air-oxidized Si(1 1 1)-(7 × 7) surfaces: Influence of short-range order on the substrate. *Appl. Surf. Sci.* **2012**, *258*, 2255–2265.
- (67) Chen, R. X.; Zhu, S. L.; Mao, J.; Cui, Z. D.; Yang, X. J.; Liang, Y. Q.; Li, Z. Y. Synthesis of CuO/Co<sub>3</sub>O<sub>4</sub> Coaxial Heterostructures for Efficient and Recycling Photodegradation. *Int. J. Photoenergy* **2015**, *2015*, 183468.
- (68) Kester, E.; Gillot, B.; Perriat, P.; Dufour, P.; Villette, C.; Tailhades, P.; Rousset, A. Thermal Behavior and Cation Distribution of Submicron Copper Ferrite Spinel Cu<sub>x</sub>Fe<sub>3-x</sub>O<sub>4</sub> (0 < x < 0.5) Studied by DTG, FTIR, and XPS. *J. Solid State Chem.* **1996**, *126*, 7–14.
- (69) Biesinger, M. C. Advanced Analysis of Copper X-Ray Photoelectron Spectra. *Surf. Interface Anal.* **2017**, *49*, 1325–1334.
- (70) Biesinger, M. C.; Lau, L. W. M.; Gerson, A. R.; Smart, R. S. C. Resolving Surface Chemical States in XPS Analysis of First Row Transition Metals, Oxides and Hydroxides: Sc, Ti, V, Cu and Zn. *Appl. Surf. Sci.* **2010**, *257*, 887–898.
- (71) Arellano, U.; Shen, J. M.; Wang, J. A.; Timko, M. T.; Chen, L. F.; Vázquez Rodríguez, J. T.; Asomoza, M.; Estrella, A.; González Vargas, O. A.; Llanos, M. E. Dibenzothiophene Oxidation in a Model Diesel Fuel Using CuO/GC Catalysts and H<sub>2</sub>O<sub>2</sub> in the Presence of Acetic Acid under Acidic Condition. *Fuel* **2015**, *149*, 15–25.
- (72) Wang, Y.; Qu, F.; Liu, J.; Wang, Y.; Zhou, J.; Ruan, S. Enhanced H<sub>2</sub>S Sensing Characteristics of CuO-NiO Core-Shell Microspheres Sensors. *Sens. Actuators, B* **2015**, *209*, 515–523.
- (73) Chastain, J. *Handbook of X-Ray Photoelectron Spectroscopy*; Moulder, J. F.; Stickle, W. F.; Sobol, P. E.; Bomben, K. D. Eds.; Perkin-Elmer Corp; Phys. Electron. Div. 1992.
- (74) Zuo, Z.-J.; Li, J.; Han, P.-D.; Huang, W. XPS and DFT Studies on the Autooxidation Process of Cu Sheet at Room Temperature. *J. Phys. Chem. C* **2014**, *118*, 20332–20345.
- (75) Benito, N.; Palacio, C. Mixed Ti-O-Si Oxide Films Formation by Oxidation of Titanium-Silicon Interfaces. *Appl. Surf. Sci.* **2014**, *301*, 436–441.
- (76) Istratov, A. A.; Flink, C.; Hieslmaier, H.; Weber, E. R.; Heiser, T. Intrinsic Diffusion Coefficient of Interstitial Copper in Silicon. *Phys. Rev. Lett.* **1998**, *81*, 1243–1246.
- (77) McBrayer, J. D.; Swanson, R. M.; Sigmon, T. W. Diffusion of Metals in Silicon Dioxide. *J. Electrochem. Soc.* **1986**, *133*, 1242.
- (78) Valladares, L. D. L. S.; Salinas, D. H.; Dominguez, A. B.; Najarro, D. A.; Khondaker, S. I.; Mitrelias, T.; Barnes, C. H. W.; Aguiar, J. A.; Majima, Y. Crystallization and Electrical Resistivity of Cu<sub>2</sub>O and CuO Obtained by Thermal Oxidation of Cu Thin Films on SiO<sub>2</sub>/Si Substrates. *Thin Solid Films* **2012**, *520*, 6368–6374.
- (79) Shin, D.-W.; Wang, S. X.; Marshall, A. F.; Kimura, W.; Dong, C.; Augustsson, A.; Guo, J. Growth and Characterization of Copper Nanoclusters Embedded in SiC Matrix. *Thin Solid Films* **2005**, *473*, 267–271.
- (80) Uchinokura, K.; Sekine, T.; Matsuhara, E. Raman Scattering By Silicon. *Solid State Commun.* **1972**, *11*, 47–49.
- (81) Cowley, R. A. Raman Scattering from Crystals of the Diamond Structure. *J. Phys. France* **1965**, *26*, 659–667.
- (82) Dolling, G.; Cowley, R. A. The thermodynamic and optical properties of germanium, silicon, diamond and gallium arsenide. *Proc. Phys. Soc.* **1966**, *88*, 463.
- (83) Choudhary, S.; Sarma, J. V. N.; Pande, S.; Ababou-Girard, S.; Turban, P.; Lepine, B.; Gangopadhyay, S. Oxidation Mechanism of Thin Cu Films: A Gateway towards the Formation of Single Oxide Phase. *AIP Adv.* **2018**, *8*, No. 055114.
- (84) Zheng, Z.; Wu, H.-H.; Chen, H.; Cheng, Y.; Zhang, Q.; Xie, Q.; Wang, L.; Zhang, K.; Wang, M.-S.; Peng, D.-L.; Zeng, X. C. Fabrication and Understanding of Cu<sub>3</sub>Si-Si@carbon@graphene Nanocomposites as High-Performance Anodes for Lithium-Ion Batteries. *Nanoscale* **2018**, *10*, 22203–22214.
- (85) Thermadam, S. P.; Bhagat, S. K.; Alford, T. L.; Sakaguchi, Y.; Kozicki, M. N.; Mitkova, M. Influence of Cu Diffusion Conditions on the Switching of Cu-SiO<sub>2</sub>-Based Resistive Memory Devices. *Thin Solid Films* **2010**, *518*, 3293–3298.
- (86) Zhou, F.; Szczech, J.; Pettes, M. T.; Moore, A. L.; Jin, S.; Shi, L. Determination of Transport Properties in Chromium Disilicide Nanowires via Combined Thermoelectric and Structural Characterizations. *Nano Lett.* **2007**, *7*, 1649–1654.

(87) Mattheiss, L. F. Structural Effects on the Calculated Semiconductor Gap of CrSi<sub>2</sub>. *Phys. Rev. B* **1991**, *43*, 1863.